Published in final edited form as:
Biochemistry. 2000 November 14; 39(45): 13760–13771.

Identification of the Cu^{2+} Binding Sites in the N-Terminal Domain of the Prion Protein by EPR and CD Spectroscopy†

Eliah Aronoff-Spencer[‡,§,‖], **Colin S. Burns**[‡,§], **Nikolai I. Avdievich**[‖], **Gary J. Gerfen**[‖], **Jack Peisach**[‖], **William E. Antholine**[⊥], **Haydn L. Ball**[#,♦], **Fred E. Cohen**[⊗,+,○,♦], **Stanley B. Prusiner**[#,⊗,♦], and **Glenn L. Millhauser**[*,§]

[§]Department of Chemistry and Biochemistry, UniVersity of California, Santa Cruz, California 95064

[‖]Department of Physiology and Biophysics, Albert Einstein College of Medicine, 1300 Morris Park AVenue, Bronx, New York 10461

[⊥]Biophysics Research Institute, Medical College of Wisconsin, Milwaukee Wisconsin 53226

[#]Department of Neurology, University of California, San Francisco, California 94143

[⊗]Department of Biochemistry and Biophysics, University of California, San Francisco, California 94143

[+]Department of Cellular and Molecular Pharmacology, University of California, San Francisco, California 94143

[○]Department of Medicine, University of California, San Francisco, California 94143

[♦]Institute for Neurodegenerative Disease, University of California, San Francisco, California 94143

Abstract

Recent evidence indicates that the prion protein (PrP) plays a role in copper metabolism in the central nervous system. The N-terminal region of human PrP contains four sequential copies of the highly conserved octarepeat sequence PHGGGWGQ spanning residues 60–91. This region selectively binds divalent copper ions (Cu^{2+}) in vivo. To elucidate the specific mode and site of binding, we have studied a series of Cu^{2+}–peptide complexes composed of 1-, 2-, and 4-octarepeats and several sub-octarepeat peptides, by electron paramagnetic resonance (EPR, conventional X-band and low-frequency S-band) and circular dichroism (CD) spectroscopy. At pH 7.45, two EPR active binding modes are observed where the dominant mode appears to involve coordination of three nitrogens and one oxygen to the copper ion, while in the minor mode two nitrogens and two oxygens coordinate. ESEEM spectra demonstrate that the histidine imidazole contributes one of these nitrogens. The truncated sequence HGGGW gives EPR and CD that are indistinguishable from the dominant binding mode observed for the multi-octarepeat sequences and may therefore comprise the fundamental Cu^{2+} binding unit. Both EPR and CD titration experiments demonstrate rigorously a 1:1 Cu^{2+}/octarepeat binding stoichiometry regardless of the number of octarepeats in a given peptide sequence. Detailed spin integration of the EPR signals demonstrates that all of the bound Cu^{2+} is detected thereby ruling out strong exchange coupling that is often found when there is imidazolate bridging between paramagnetic metal centers. A model consistent with these data is proposed in which Cu^{2+} is bound to the nitrogen of the histidine imidazole side chain and to two nitrogens from sequential glycine backbone amides.

†This work was supported by NIH Grants GM46870 (G.L.M.), GM60609 (G.J.G.), GM40168 (J.P.), and AG05830 (C.S.B.).

*To whom correspondence should be addressed. Telephone: (831) 459-2176. Fax: (831) 459-2935; glennm@hydrogen.ucsc.edu.
‡These authors made equal contributions to this work.

Prion diseases are fatal, neurodegenerative disorders in which the pathogenic agent is an isoform of a monomeric, membrane-anchored glycoprotein called the prion protein (PrP^C).[1] Conversion of PrP^C to the multimeric, protease-resistant scrapie isoform (PrP^{Sc}) is the key pathogenic event (1–3). Fundamental questions remain concerning the physiological role of PrP^C, the mechanism leading to formation of PrP^{Sc}, and the neurotoxocity of this misfolded species.

The tertiary structures of recombinant unglycosylated human, mouse, and hamster PrP^C have been determined by NMR (4–8). Under the conditions used in these NMR studies, the N-terminal portion of mature PrP^C, residues 23–125, is largely unstructured in solution while the C-terminal segment, residues 126–231, shows considerable structure, including three α-helices and two small β-strands. Purification of PrP^C from brain homogenates reveals the full-length mature glycosylated and glycosylphosphatidylinositol-anchored (GPI) structure (residues 23–231) suggesting that residues 23–125 are likely to adopt a more ordered structure in vivo thereby avoiding additional proteolytic processing (9). The precise tertiary and quaternary structure of PrP^{Sc} is unknown, but spectroscopic studies show that it possesses high β-sheet content as well as residual helical structure (9,10).

Recent evidence indicates that PrP^C may play a role in copper homeostasis (11–13). A number of studies have demonstrated that N-terminal fragments of PrP^C and the full-length protein bind divalent copper (Cu^{2+}) (11,14–19) and do so preferentially over other divalent metal ions (14,15,19). The N-terminal region of human PrP^C contains four sequential copies of a highly conserved octarepeat sequence P**H**GGGWGQ spanning residues 60–91 (20,21). The high histidine content of this region suggests that it may be involved in metal ion binding (22). Spectroscopic studies have shown that Cu^{2+} induces ordered structure in the regions of PrP^C previously thought to be flexible by NMR spectroscopy (15).

Three models of the Cu^{2+} binding mode in PrP^C have been put forth based on spectroscopic studies. According to Stöckel et al. (15), who studied recombinant unglycosylated PrP(23–231) and various PrP fragments, at pH 6 two histidyl imidazole nitrogens and two glycine carbonyls from adjacent octarepeat units bind a single Cu^{2+}. Viles et al. (17) observed cooperative binding in a variety of octarepeat containing PrP fragments. This led to the proposal that at just above pH 7, PrP(58–91) binds Cu^{2+} through a ring-like structure composed of four metal ions and four bridging imidazolate ions. Alternatively, Raman studies by Miura et al. (16,18) on single and multi-octarepeat containing peptides suggest that each octarepeat independently binds Cu^{2+} and that the minimum binding unit is the HGGG segment of the octarepeat. Here, the N_π nitrogen (also denoted Nδ1) of the imidazole and the amide nitrogens of the last two glycine residues coordinate Cu^{2+}.

While each study proposes a different structural model, there is good agreement regarding the Cu^{2+} to octarepeat binding stoichiometry. All work to date on N-terminal segments above pH 7 show that the stoichiometry is 1:1 Cu^{2+}/octarepeat (11,14,16–18) with the exception that Viles et al. find that PrP(51–75) and PrP(73–91), each of which contains two octarepeat units, bind a single copper ion (17). Stöckel et al. find that, below pH 7, in full PrP two octarepeats are necessary to bind a single Cu^{2+} ion.

Given that the octarepeat repeat is highly conserved among mammalian PrP proteins, and further that PrP binds Cu^{2+} in vivo (11), strongly suggests that this region plays a physiological

[1]Abbreviations: PrP, prion protein; PrP^C, cellular isoform of PrP; PrP^{Sc}, scrapie isoform of PrP; PrP(57–91), residues 57 through 91 of PrP; EPR, electron paramagnetic resonance; ESEEM, electron spin–echo envelope modulation; e^2qQ/h, maximum quadrupole coupling; η, quadrupole asymmetry parameter; CD, circular dichroism; NMR, nuclear magnetic resonance; GPI, glycosylphosphatidylinositol; SOD, superoxide dismutase; ESI-MS, electrospray ionization mass spectrometry; NEM, *N*-ethylmorpholine; K_d, dissociation constant.

or structural role. Efforts to determine the precise function of PrP are ongoing (13,23–25). Brown et al. (23) have shown that PrP^C folded in the presence of Cu^{2+} exhibits superoxide dismutase (SOD) activity and may serve to protect synaptic regions from oxidative stress. However, PrP^C is continuously recycled through endocytosis and, thus, an alternative proposal is that the role of PrP^C is to shuttle Cu^{2+} from the synaptic space to the cell interior (13,19, 25). Indeed, recent work suggests that Cu^{2+} stimulates endocytosis of PrP (13) and, further, that PrP may release Cu^{2+} in the low pH environment of endosomes (19). Characterization of the Cu^{2+} binding site and evaluation of whether such a binding site will be pH-sensitive in vivo are essential for clarifying PrP's physiological function.

Divalent copper is a d^9 metal ion and is readily observable by electron paramagnetic resonance. We report an EPR study detailing the magnetic properties of copper-bound peptide fragments corresponding to one, two, and four PrP octarepeats and a series of six peptides that are shortened or frame-shifted (with respect to the octarepeat peptide sequence) analogues of the conserved octarepeat unit. In addition, a peptide of four octarepeats where the tryptophan side chains were replaced with cyclohexylalanine, a bulky nonaromatic residue, was examined. pH titrations followed by EPR show that Cu^{2+} is bound at pH values greater than 5. At pH 7.4, the 1, 2, and 4 peptide repeats have nearly identical EPR spectra indicating that the mode of binding is similar in all three. Two EPR active binding modes were observed. The dominant mode appears to involve coordination of three nitrogens and one oxygen to the copper ion. This is supported by S-band EPR which directly reveals ^{14}N superhyperfine couplings. ESEEM spectra demonstrate that one of the nitrogens is from the histidine imidazole. EPR spectra of Cu^{2+} bound **H**GGGW, corresponding to only five residues of the octarepeat, suggests that this peptide is the minimum unit capable of mimicking the dominant coordination environment of the octarepeat and longer N-terminal peptides. However, EPR of Cu^{2+} bound to peptide **H**GG reveals the existence of both binding modes, and this sequence may therefore contain the nitrogens that directly bind copper. CD spectra obtained in the visible region corresponding to the d–d transitions revealed only small variations of the associated λ_{max} values. The stoichiometry of Cu^{2+} binding was determined using both EPR and CD spectroscopy and, consistent with previous studies, demonstrates that the Cu^{2+}/octarepeat stoichiometry is 1:1. Finally, EPR spin quantitation of the signal arising from Cu^{2+} bound to a four octarepeat peptide suggests that all of the bound copper ion is detected. This finding is of relevance when considering proposed structures containing bridging imidazolates since such bridging results in a reduction of the EPR signal.

MATERIALS AND METHODS

Peptide Synthesis and Purification

PrP(57–91), PrP(23–28, 57–91), PrP(23–28, 57–91 W → X), and PrP(73–91) were synthesized at UCSF. All other peptides were prepared at UCSC by solid-phase synthesis using standard fluorenylmethoxycarbonyl (Fmoc) methods. Peptides were acetylated at the N-terminus and amidated at the C-terminus. Finally, all peptides were purified using reverse phase HPLC and characterized by electrospray ionization mass spectrometry (ESI-MS) (VG Quattro II, Fisons Instruments).

Peptide Sample Preparation and Concentration Determination

All peptide solutions were made in a degassed buffer containing 25 mM *N*-ethylmorpholine (NEM), 150 mM potassium chloride (KCl), and 20% glycerol (v/v) where the glycerol served as a cryoprotectant. The pH of the solution was adjusted to the desired value using a concentrated hydrochloric acid (HCl) or potassium hydroxide (KOH) solution. This buffer was used for all studies except where otherwise indicated. Peptide concentrations were determined by acquiring UV–Vis spectra of samples in 6 M guanidine hydrochloride. The extinction

coefficient for tryptophan at 280 nm, which was taken to be 5609 M^{-1} cm^{-1}, was used to calculate the peptide concentration.

All samples for EPR experiments, with the exception of those used for Cu^{2+} titrations, were prepared with $^{63}CuCl_2$ (99.62%, Cambridge Isotope Laboratories). The pure isotope ^{63}Cu was used to avoid inhomogeneous broadening of the EPR lines that would otherwise be present with the mixture of naturally occurring isotopes ^{63}Cu and ^{65}Cu.

Electron Paramagnetic Resonance (EPR) and Electron Spin–Echo Envelope Modulation Spectroscopy (ESEEM)

X-Band EPR spectra (9.43 GHz) were acquired using a Bruker ESP380 spectrometer and a TE_{102} cavity equipped with variable temperature control. Unless otherwise specified, all X-band EPR spectra were acquired at 77 K. Spectra at liquid helium temperatures were acquired using a dielectric resonator (9.73 GHz). S-band spectra (3.5 GHz) were acquired at 133 K using a loop gap resonator as part of a specially designed spectrometer housed at the Biomedical ESR Center at the Medical College of Wisconsin. The $m_I = -1/2$ lines of these spectra were simulated using stick diagrams with Gaussian line shapes. Three pulse ESEEM measurements were obtained at 4.2 K on an X-band pulsed-EPR spectrometer. The instrument, cavity, and resonator were constructed in-house and have been previously described (26,27). Continuous wave spectra were first acquired on a Varian E-112 X-band spectrometer. Data were then obtained at $g_\perp$, the point of greatest spectral intensity (3315 G at 9.47 GHz). The ESEEM acquisition parameters were $\tau = 150$ ns, starting $T = 40$ ns, a time increment of 20 ns, and a repetition rate of 53 Hz. Data processing to attain frequency domain spectra was carried out using software described in previous work (28).

Circular Dichroism (CD) Spectroscopy

CD spectra were acquired on an Aviv 60DS spectrometer at 298 K. A 1-cm path length cell was used for spectra recorded between 350 and 800 nm sampling points every 1 nm.

Titration with Cu^{2+}

Copper titrations were monitored by EPR at 77 and 298 K and by CD at 298 K. Solutions of Cu^{2+} were made from $CuCl_2$ such that 5-μL additions would deliver the equivalents of copper necessary for the given titration. The pH of the copper stock was adjusted to 7.4 so that the pH of the peptide solution would not drop during the titration due to the addition of the Cu^{2+} solution. Copper concentrations were determined by comparison to standard solutions containing known amounts of Cu^{2+} in 10 mM imidazole at pH 7.4. Foldover concentrations, which were used to determine the binding equivalence, were determined by fitting the low and high [Cu^{2+}] regions of the curve to a linear function and then evaluating the point of intersection.

RESULTS

EPR and CD

The peptide segment PrP(57–91) contains four repeats of the conserved sequence P**H**GGGWGQ and corresponds to the main N-terminal copper binding region as suggested by other studies (14,15). Our strategy focused on examining a series of peptide segments derived from PrP-(57–91) to determine the structural elements necessary for Cu^{2+} binding. Table 1 displays all peptides investigated. Several of the sequences contain the string of basic residues KKRPKP at their N-termini corresponding to PrP(23–28). As will be discussed further below, addition of this sequence increased solubility in aqueous solution which, in turn, facilitated spectroscopic measurements. All of the peptides are composed of only standard L-amino acids

with the exception of PrP(23–28, 57–91 W → X) where all tryptophan side chains were substituted with the nonaromatic cyclohexylalanine moiety. This peptide was included to explore the role of the indole side chain in Cu^{2+} coordination. All peptides listed below the octarepeat in Table 1 are truncated and/or frame-shifted analogues of this basic unit. Finally, all peptides were chemically blocked with an acetyl group (Ac) at the N-terminus and an -NH_2 group at the C-terminus. Blocking the N-terminus was important since polypeptide N-terminal amines can bind directly to copper ions.

It is well-established that Cu^{2+}/peptide interactions are strongly pH-dependent. The X-band EPR spectra of PrP-(23–28, 57–91) with 4 equiv of ^{63}Cu are shown in Figure 1 at several pH values between 4 and 12. Figure 1 shows that as the pH is increased there are marked changes of the four hyperfine lines in the low field, parallel region of the spectrum. (Note, the four lines in this region arise from hyperfine coupling to the $I = 3/2$ ^{63}Cu nucleus.) Specifically, $g_{\|}$ and $A_{\|}$ shift, and this is readily ascribable to changes in the ligand environment around the copper ion (29). Figure 2 shows an expansion of this low field region at selected pH values. At pH 4.10, the spectrum has four dominant lines with $g_{\|} = 2.41$ and $A_{\|} = 408$ MHz (121 G), which is characteristic of aqueous copper. This aquo signal suggests there is no detectable binding between Cu^{2+} and peptide at this pH. At pH 5.30, a new set of lines appear corresponding to a spectrum with $g_{\|} = 2.37$ and $A_{\|} = 415$ MHz (125 G). According to established Peisach–Blumberg correlations, these values clearly fall in the range expected for coordination of a single nitrogen ligand and three oxygen ligands in the equatorial plane (29). The observation that binding begins to occur near pH 6 supports previous suggestions that histidine is involved in complexing Cu^{2+} (15–18). Increasing the pH to 6.75, the spectrum is now composed of two sets of lines with values $g_{\|} = 2.27$, $A_{\|} = 537$ MHz (169 G) and $g_{\|} = 2.23$, $A_{\|} = 493$ MHz (158 G), respectively. At pH 8.57, only the latter spectrum is observed. Both of these spectra are consistent with binding of 2–3 nitrogen ligands. Finally, at pH 11.60, only one species is observed with $g_{\|} = 2.20$ and $A_{\|} = 582$ MHz (189 G), which is consistent with binding to four nitrogen ligands. Magnetic parameters derived from these spectra are summarized in Table 2.

Returning to Figures 1 and 2, the spectrum obtained at pH 7.45 shows that the dominant copper bound PrP(23–28, 57–91) species is the same as that observed at pH 8.57. We refer to this spectrum as component 1 (Figure 2). Also, the lines observed at pH 6.75 are still present as a minor spectral component at pH 7.45, demonstrating that at least one other binding mode is present. We refer to this second spectrum as component 2. As noted above, component 1 and component 2 spectra are not absolutely definitive with respect to the number of bound nitrogens based on magnetic parameters alone. However, given that nitrogen ligation in peptide–Cu^{2+} complexes increases with elevated pH, we assign component 1 as arising from coordination with three nitrogens and one oxygen and component 2 arising from coordination with two nitrogens and two oxygens.

Figure 3 displays the EPR spectra of all the peptides with excess $^{63}Cu^{2+}$ at pH 7.45 ± 0.07. Excess copper was used to ensure that all peptides were fully loaded with metal ion. At pH ≥ 7, aquo Cu^{2+} is only sparingly soluble and precipitates as EPR silent $[Cu(OH)_2]_n$, and hence the excess of Cu^{2+} does not introduce interference from the aquo species. The spectrum of PrP (57–91) is shown at the top of Figure 3. This peptide was less soluble than PrP(23–28, 57–91) when bound as a copper complex and signal averaging was required to obtain a high quality spectrum. (Note: this sample contained less than 100 μM peptide.) The splitting between the $m_I = -1/2$ and $m_I = +1/2$ hyperfine lines serves as a diagnostic for assessing $g_{\|}$ and $A_{\|}$, and thus two vertical lines passing through these features of component 1 have been added to Figure 3 to aid in comparison of the spectra. The spectrum obtained from PrP(57–91) is nearly identical to that of PrP(23–28, 57–91) with all the transitions appearing in the same positions with similar intensity ratios. The Cu^{2+}/peptide system PrP(23–28, 57–91 W → X) also produces a spectrum where the main hyperfine lines are nearly superimposable with Prp(23–28, 57–91). The

similarity observed between PrP(23–28, 57–91) and PrP(23–28, 57–91 W → X) suggests that the indole side chain has minimal influence on the environment of the paramagnetic electron.

The peptides PrP(73–91) and PrP(23–28, 73–91), containing two octarepeats, give spectra nearly identical to that of PrP(57–91). One interesting feature unique to these two sequences and PrP(23–28, 57–91) is a new component in the high field region of the spectrum at approximately 3500 G. The origin of this feature is not clear but could arise from dipolar coupling between closely spaced copper ions (30).

The octarepeat unit itself, P**H**GGGWGQ, and the frame-shifted analogue GQP**H**GGGW reproduce the spectral features observed for both PrP(57–91) and PrP(23–28, 57–91). The next system, GQP**H**GGG, which does not contain the tryptophan residue, reveals a change in the spectrum. As compared to PrP(57–91) and PrP(23–28, 57–91), component 2 is more pronounced. Comparing this spectrum to that obtained from the octarepeat suggests that a residue following the **H**GGG unit helps structure the coordination environment.

The peptides **H**GGGWG and **H**GGGW represent substantial reduction of the fundamental octarepeat sequence. Interestingly, spectra obtained from these peptides reproduce the spectral features of PrP(57–91). However, further reduction to **H**GGG yields a pronounced difference when compared to the octarepeat. Specifically, now component 2 dominates the spectrum. Finally, the tripeptide **H**GG exhibits approximately the same spectrum as **H**GGG. (When preparing Cu^{2+} complexes from these small peptides sufficient Cu^{2+} was added to ensure that the copper ion was bound by only a single peptide molecule, and this was verified with quantitative spin integration for **H**GGGW and all longer peptides. Thus, formation of dimeric species where two peptide molecules bind a single Cu^{2+} was avoided.)

Magnetic parameters obtained from the spectra in Figure 3 are reported in Table 3. Parameters for component 1 reveal little variation, although $A_{\|}$ is slightly reduced for those peptides without a residue following the **H**GGG segment. Parameters for component 2 spectra could only be reliably obtained for three of the peptides, but again variation among this set is small. Given that **H**GGGW is the shortest peptide to give only a component 1 spectrum suggests that this segment binds Cu^{2+} in a fashion equivalent to the longer multi-octarepeat peptides and therefore comprises the fundamental binding unit.

PrP(57–91) was further analyzed to test for the presence of any coupled copper species. The half-field region of the spectrum was scanned for the $\Delta M = 2$ transition that is often observed in the spectra of spin coupled complexes. No $\Delta M = 2$ transition was found. EPR spectra were also collected at several temperatures down to 4 K, and again there was no evidence of a $\Delta M = 2$ transition. Finally, we note that all copper could be accounted for by spin quantitation, and this will be discussed further below.

When Cu^{2+} is added to the peptides, CD bands arising from weakly allowed d–d transitions appear in the visible region. These transitions become observable by CD only when Cu^{2+} is in a chiral ligand environment, and thus trace amounts of aqueous copper ion are not detected. The CD spectra for the peptides at pH 7.4 are shown in Figure 4. For the systems PrP(23–28, 57–91), PrP(73–91), and PrP-(23–28, 73–91), these transitions are centered roughly at 650 nm with a positive band near 580 nm and a negative band near 700 nm. [Poor solubility of the copper complex of PrP(57–91) prohibited the acquisition of a CD spectrum with an acceptable signal-to-noise ratio, and thus it is not included in Figure 4.] The single octarepeat and all systems equal in size or smaller exhibit transitions centered at approximately 665 nm with positive bands near 600 nm and negative bands near 720 nm. The peptide PrP(23–28, 57–91 W → X) has CD characteristics that fall between those of the large and small systems with the transition centered at approximately 662 nm and positive and negative bands at 595 and 724

nm, respectively. An additional positive band is apparent at 340 nm for all copper/peptide complexes studied here (not shown).

Absorption bands due to d–d transitions can arise over a range of wavelengths from 500 to 750 nm. Transition pairs arising specifically between 570 and 750 nm are consistent with tetragonally distorted five- or six-coordinate Cu^{2+} with nitrogen ligands. It is interesting to note that while the EPR shows a clear difference between **H**GGGW, the proposed fundamental binding unit, and the shorter sequences **H**GGG and **H**GG, the optical transitions are indistinguishable. It appears that these short peptides all bind mainly through nitrogen coordination, but there are subtle differences in the local coordination geometry that is reflected mainly in the EPR spectra. The subtle shift of approximately 20 nm observed in the transitions when comparing the short peptides to the longer multi-octarepeat sequences is very small but may reflect somewhat greater tetragonal distortion for the longer sequences.

Cu^{2+} Titrations Followed by EPR and CD

EPR and CD signals were obtained as a function of titrated Cu^{2+} to determine metal ion to octarepeat binding stoichiometry. Our interest was in determining whether the stoichiometry differs between the octarepeat and the multi-octarepeat sequences. We therefore focused solely on the single octarepeat, PrP-(23–28, 73–91) with two octarepeats, and PrP(23–28, 57–91) with four octarepeats.

The positive CD signal intensity was followed as a function of added Cu^{2+} at pH 7.4. The titration curves for the octarepeat, PrP(23–28, 73–91), and PrP(23–28, 57–91) are shown in Figure 5. Peptide concentrations were between 50 and 400 μM and copper ion concentrations reported in equivalents per peptide (see Figure 5 for exact concentration of each peptide). Figure 5 shows that the CD band increases and folds over at 1.1 ± 0.2, 2.5 ± 0.5, and 4.4 ± 0.8 equiv of added copper for the three peptides, respectively. Interestingly, the titration curve for the octamer increases linearly, whereas the curves for both PrP(23–28, 73–91) and PrP(23–28, 57–91) show curvature in the region of 1.0 added equivalent. This is discussed further below. The maximum positive molar ellipticity was 2180 deg cm^2 $dmol^{-1}$ for the octarepeat unit, 4370 deg cm^2 $dmol^{-1}$ for PrP(23–28, 73–91), and 7572 deg cm^2 $dmol^{-1}$ for PrP-(23–28, 57–91). Normalizing such that the maximum positive molar ellipticity reached for the octarepeat unit is defined as 1.0 equiv of Cu^{2+}, PrP(23–28, 73–91), and PrP-(23–28, 57–91) are found to bind approximately 2.0 and 4.2 equiv of Cu^{2+}, respectively. Thus, CD signal titration and maximal signal intensity both demonstrate that the Cu^{2+}/octarepeat stoichiometry is 1:1 regardless of the number of octarepeats in a given peptide. These results are summarized in Table 4.

Double integration of first derivative EPR spectra was used to quantitate the amount of titrated Cu^{2+} at pH 7.4. Peptide concentrations were in the range of 250 to 1000 μM, and again the copper ion concentration is reported in equivalents per peptide. Results for the octarepeat, PrP (23–28, 73–91), and PrP(23–28, 57–91) are shown in Figure 6. The titration curves for these three systems all increase linearly and fold over at 0.9 ± 0.2, 1.9 ± 0.4, and 4.2 ± 0.8 equiv of added copper, respectively. The absolute concentration of bound Cu^{2+} was determined by spin integration followed by comparison to a copper standard. Quantitated in this manner, octamer, PrP(23–28, 73–91), and PrP(23–28, 57–91) bind 0.8 ± 0.1, 1.9 ± 0.3, and 3.8 ± 0.6 equiv of copper, respectively. These data agree with the CD results and again demonstrate a 1:1 Cu^{2+}/ octarepeat stoichiometry (see Table 4).

Returning to the CD titration in Figure 5, it was noted that the titration curves for both PrP(23–28, 73–91) and PrP(23–28, 57–91) are curved at low Cu^{2+} concentration, whereas for the octarepeat it is linear. Specifically, with 1 equiv of Cu^{2+}, PrP(23–28, 57–91) gives a very weak CD signal relative to the octamer. In contrast, the EPR signal integrals in Figure 6 show that all added Cu^{2+} is bound in this same respective region of the titration curve. Affinities have

been determined for PrP–Cu^{2+} complexes, and the dissociation constants (K_d) range from 1 to 5 μM. Accordingly, at the concentrations used for the CD and EPR titrations (>150 μM in octarepeat concentration), greater than 85% of the Cu^{2+} should be bound in a 1:1 complex, and this is consistent with the EPR titration data and the CD titration of the octamer. Thus, the weak CD signal at 1.0 equiv of Cu^{2+} observed for the longer complexes arises not from lack of association to form the peptide–Cu^{2+} complex but instead a molecular environment that exhibits lower CD activity than that of the octamer–Cu^{2+} complex. That this curvature exists only for the multi-octarepeat sequences argues that at low Cu^{2+} concentration there is a coordination environment that differs from that observed in the fully bound complexes. To test for this possibility, we examined EPR spectra of PrP(23–28, 57–91) at various Cu^{2+} concentrations, and the results are shown in Figure 7. Spectra are normalized such that the integrals are equal. Indeed, at 1 and 2 equiv, the spectra are markedly different than that observed at 4 equiv. The spectral features of the dominant species at 1 equiv (arrows) are similar to the component 2 spectra of Figure 3, perhaps suggesting that two nitrogens coordinate at low Cu^{2+} concentrations. Viles et al. have suggested that two His side chains may bind to the metal ion centers at low Cu^{2+} concentrations, and this may explain the results of Figure 7 (17) and the cooperative nature of Cu^{2+} binding (11,19). How the coordination environment changes as a function of Cu^{2+} concentration is an issue of considerable importance given biological concentrations of Cu^{2+} (11), PrP (31), and other copper binding species.

ESEEM and S-Band EPR

Three pulse electron spin–echo envelope modulation (ESEEM) spectroscopy (32,33) was performed to aid in the characterization of the Cu^{2+} coordination environment. Spectra for fully Cu^{2+} loaded PrP-(23–28, 57–91), octarepeat, and **H**GGGW are shown in Figure 8. PrP (23–28, 57–91) is less soluble than the other two peptides thereby accounting for the relative reduction in the signal-to-noise of its ESEEM spectrum. All three spectra are quite similar and are dominated by features that are consistent with coordination by the histidine imidazole. Specifically, the low-frequency lines at 0.59, 0.87, and 1.47 MHz are characteristic of a weakly coupled ^{14}N close to the exact cancellation limit (33,34). This limit corresponds to a zero vector sum of the ^{14}N nuclear Zeeman and hyperfine fields in one of the electron spin manifolds and thus gives rise to nearly pure ^{14}N quadrupolar transitions. These frequencies yield the quadrupolar parameters $|e^2Qq/h| = 1.56$ MHz and $\eta = 0.75$ (26). The values of these parameters and the observed ESEEM frequencies are typical of that observed for the remote, noncoordinated nitrogen of an imidazole ring bound to Cu^{2+} (26). In addition, the broad features at approximately 4 MHz arise from the $\Delta m_I = 2$ transitions taking place within the other electron spin manifold (26,33).

The ESEEM spectra in Figure 8 are typical for Cu^{2+} coordinated by imidazole and thus support the assignment here and in other works (14,15,17,18) that the histidine side chain participates in the coordination environment. ESEEM spectra can also be used to assess the number of histidines bound to the copper center. Specifically, when two or more imidazoles coordinate to a single Cu^{2+}, the $\Delta m_I = 2$ signal is enhanced and accompanied by combination peaks arising at multiples of the fundamental low frequency (<2 MHz) transitions (35). The relative amplitude of the $\Delta m_I = 2$ transition for PrP(23–28, 57–91) does not appear to be enhanced when compared to the same transition for the octarepeat and **H**GGGW. Furthermore, ESEEM of PrP(23–28, 57–91) does not reveal evidence of combination peaks between 2 and 3 MHz. Hence, these ESEEM spectra suggest that each octarepeat within PrP(23–28, 57–91) contributes a single imidazole to its coordinated Cu^{2+}.

The values of the nuclear quadrupolar transitions also identify the protonation state of the remote nitrogen. The remote nitrogen of neutral imidazole gives rise to Cu^{2+} ESEEM spectra with sharp transitions below 2 MHz as observed here. Deprotonated imidazole (e.g.,

imidazolate) gives transitions at approximately 0.24 MHz, 2.34 MHz, and 2.58 ($|e^2qQ/h| \approx$ 3.28 MHz, $\eta \approx 0.15$) (33) and thus cannot account for dominant ESEEM transitions for the three peptides in Figure 8. Finally, transitions at 2.00 and 2.85 MHz are observed for the octarepeat and **H**GGGW. At this juncture, the origin of these transitions is not clear; however, they do not appear to arise from combinations of the lower frequency components. In addition, Cu^{2+} titration experiments with the octarepeat (Figures 5 and 6) demonstrate a 1:1 Cu^{2+} to peptide stoichiometry thereby ruling out multiple histidine coordination in these short peptides. It is possible that these peaks arise from other noncoordinated nitrogens within the **H**GGGW binding unit. Interestingly, these transitions are not clearly observed for PrP(23–28, 57–91). Perhaps subtle variations in the octarepeat structures within this four octarepeat peptide results in variations of these frequencies thereby broadening and reducing the relative amplitude of these lines. Aside from these two unassigned components, these ESEEM data suggest that the imidazoles in all three peptides exist in similar chemical environments and clearly participate in Cu^{2+} coordination.

Analysis of the component 1 EPR spectra in Figures 1–3 suggests that three nitrogens participate in the equatorial coordination environment of the Cu^{2+} center in all peptides that contain the fundamental **H**GGGW segment. The next goal is to test this assignment by probing for the existence of nitrogen superhyperfine couplings. Nitrogens directly coordinated to Cu^{2+} typically give couplings between 10 and 15 G (36, 37). Unfortunately, these couplings are often masked by inhomogeneous broadening arising from *g* and *A* strain. Spectra for the octarepeat and GQP**H**GGGW in Figure 3 do exhibit subtle superhyperfine structure near the first derivative maximum at 3250 G. However, analysis of couplings in this $g_\perp$ region of the spectrum is difficult because small differences in g_{xx} and g_{yy} can complicate the multiplet structure. Another approach is to employ low frequency S-band (3.5 GHz) EPR. The benefit of S-band EPR arises from a partial cancellation of *g*-strain and *A*-strain induced inhomogeneous broadening specifically for the ^{63}Cu $m_I = -1/2$ hyperfine line (36). The S-band EPR spectrum for the octarepeat is shown in Figure 9. Because of the reduced Zeeman interaction, the ^{63}Cu hyperfine interaction now dominates the spectrum. The $m_I = -1/2$ hyperfine line reveals subtle splittings arising from superhyperfine structure as seen in the full scan (trace A). To clearly resolve the couplings, the $m_I = -1/2$ hyperfine line was selectively scanned at high resolution with signal averaging (trace B). This signal was then differentiated to give the second harmonic (trace C) which emphasizes the multiplet splitting (38). Qualitatively, the splittings are approximately 13 G, which is consistent with ^{14}N coupling from directly coordinated nitrogens. Indeed, these observed splittings are similar to that obtained from other Cu^{2+} centers with several coordinated nitrogens.

S-band EPR spectra of the ^{63}Cu $m_I = -1/2$ line are shown for the octarepeat and **H**GGGW in Figure 10. To within experimental error, the observed multiplet patterns are equivalent. Each shows a splitting pattern consisting of six or more resolved lines. Interestingly, the symmetric splitting observed at the top of the first derivative peak demonstrates that the superhyperfine multiplets arise from an even number of lines. If the multiplets were strictly from equivalent ^{14}N superhyperfine interactions, one would expect an odd multiplet pattern. For example, one ^{14}N would give three lines (1:1:1 relative intensity), and two equivalent ^{14}N's would give five lines (1:2:3:2:1 relative intensity), etc. (39). The even multiplet observed here can arise from either inequivalent ^{14}N's or an additional $I = 1/2$ spin arising from perhaps a nearby ^1H (39). In most cases, directly coordinated nitrogens do not exhibit grossly different hyperfine couplings, and, alternatively, there is good precedent for participation of several nitrogens and a proton contributing to these multiplets (40). (Note that these spectra were obtained in D_2O, so an ^1H must arise from a peptide hydrogen.) Simulations were performed assuming equivalent ^{14}N couplings (a_N) and coupling from a single ^1H (a_H). Limiting the simulations to reasonable values of these couplings, the best results were obtained from three nitrogens with $a_N = 13$ and $a_H = 10$ G. The results are shown in Figure 10. The simulated

spectrum clearly captures the features of both the derivative and second harmonic representations. The multiplet reveals eight lines, although the outermost lines are very weak as is typical of these patterns.

The multiplet pattern observed for the copper $m_I = -1/2$ component with a_N values typical of directly bound nitrogens strongly supports the suggestion of the previous section that several nitrogens participate in the component 1 Cu^{2+} coordination environment. Moreover, the values for $g_{\|}$, $A_{\|}$, and the superhyperfine couplings obtained at S-band are all readily explained by a coordination site consisting of three nitrogens. There still remains the possibility that only two nitrogens coordinate to Cu^{2+}, and this would probably require unequal a_N values to explain the multiplet patterns in Figure 10. Future work with isotopic labeling, for example, will help resolve this issue and may also help identify the hydrogen that gives rise to the additional splitting. Finally, several attempts were made to obtain superhyperfine couplings from S-band spectra of PrP(23–28, 57–91). In all cases, no couplings were observed. The $m_I = -1/2$ line was slightly broader than that obtained from the octarepeat and **H**GGGW, suggesting that inhomogeneous broadening was masking the desired multiplet pattern. Fully loaded PrP(23–28, 57–91) contains four Cu^{2+} ions (Figures 5 and 6), and, hence, weak dipolar interactions between the paramagnetic centers may contribute an additional source of inhomogeneous broadening that is not canceled in the $m_I = -1/2$ line at S-band.

DISCUSSION

The EPR spectra in Figure 3 are all composed of two spectral components: component 1, which we propose arises from coordination of three nitrogens and one oxygen, and component 2, which may arise from two nitrogens and two oxygens. Component 1 dominates all of the spectra from peptides equal to or longer than the octarepeat, although component 2 is clearly present in several of the spectra. The simple sequence **H**GGGW gives rise to an almost pure component 1 spectrum. Given the sensitivity of EPR to coordination environment (e.g., symmetry, charge, and coordinating atoms), it appears that **H**GGGW binds Cu^{2+} in a fashion that is nearly equivalent to the multi-octarepeat peptides and therefore comprises the fundamental binding unit. Thus, we propose that fully bound PrP(57–91) takes up four Cu^{2+} ions with each metal ion coordinated to the **H**GGGW unit within an octarepeat. Interestingly, the peptides lacking a residue following the **H**GGG segment and also the shortest peptide **H**GG give rise to both component 1 and 2 spectra but now with a greater population of the latter. Thus, **H**GG may provide the necessary coordinating nitrogen atoms and the remainder of the sequence out to **H**GGGW and longer controls the equilibrium between two nitrogen and three nitrogen coordination.

The pH titrations, magnetic parameters $g_{\|}$ and $A_{\|}$, ^{14}N superhyperfine couplings (from S-band EPR), and spectra from short peptides such as **H**GG argue that component 1 arises from Cu^{2+} coordination by three nitrogens. ESEEM demonstrates that the histidine imidazole contributes one of these nitrogens. The remaining two nitrogens must come from deprotonated backbone amide groups within the fundamental **H**GGGW unit. Comparable binding motifs for peptide–Cu^{2+} complexes are well-known (41,42). Given the similarity of both component 1 and component 2 spectra across the peptide series it is worthwhile considering the uniqueness of Cu^{2+} EPR spectra. Specifically, is it possible for **H**GGGW and PrP(57–91), for example, to bind Cu^{2+} with the same number of nitrogens and oxygens but with participation of different residues? A recent study on tri- and tetrapeptides partially addresses this issue. Pogni et al. examined EPR of the series **H**GG, G**H**G, and GG**H** (43). While all of these peptides bound through either three or four nitrogens depending on pH, they gave vastly different EPR spectra especially in the $g_{\perp}$ region. Apparently, placement of the His within the sequence greatly influences the coordination site symmetry which is in turn reflected in the relative values of

g_{xx} and g_{yy}. Thus, we conclude that **H**GGGW binds Cu^{2+} with a symmetry and ligand field that is equivalent to that obtained from the longer PrP peptides.

That each copper ion is bound mainly by residues within an octarepeat is further supported by titration experiments on the 1, 2, and 4 octarepeat containing peptides (Figures 5 and 6) where both EPR and CD demonstrate that the Cu^{2+}/octarepeat stoichiometry is 1:1. This finding is consistent with the results of other researchers (11, 14, 16–18) with the exception of Viles et al. who report that PrP(51–75) and PrP(73–91), both of which contain two octarepeat units, bind only one copper ion (17). Our results with PrP(23–28,73–91) demonstrate binding to 2 equiv of Cu^{2+}, and we are unable to account for the discrepancy between our data and that from Viles et al.

The EPR spectra (Figure 3) and spin integration (Figure 6, *y* axis) also address the possibility of imidazolate bridging between copper ions. To account for cooperative binding in PrP/Cu^{2+} complexes, Viles et al. proposed a novel ring structure for PrP(57–91) composed of four histidine residues bridging between four copper ions. Imidazolate bridging is well-documented in biological systems, such as Cu_2Zn_2 superoxide dismutase (44,45) and in numerous model complexes (46,47). An imidazolate bridge between a single pair of Cu^{2+} ions leads to an exchange interaction and, for typical strong coupling, the resulting EPR transitions take place solely among the two-spin triplet levels. If, in addition, the exchange interaction is large as compared to kT, the Boltzmann factor will favor the singlet ground state thereby decreasing the integrated EPR absorption signal relative to that expected from uncoupled spins. In the EPR monitored titration experiments performed on PrP(23–28, 57–91) at 298 K (Figure 6) the Cu^{2+}/octarepeat stoichiometry was found to be approximately 1:1 when determined from spin integration. Additional spin quantitation was performed on fully Cu^{2+} loaded PrP(23–28, 57–91) as a function of temperature down to 77 K (data not shown), and the calibrated signal integrals revealed no variation to within 2% random error. Hence, there is no experimental evidence of signal loss due to exchange coupling. Typical values for the exchange interaction between Cu^{2+} pairs ranges from 17 to 90 cm^{-1} (46), and such couplings will reduce the integrated signal intensity by 10 to 70%, respectively, at 77 K. We estimate that the largest possible error in signal integral is 15%, which may mask couplings as weak as 25 cm^{-1}. (Four coupled Cu^{2+} ions will lead to a comparable loss of integrated signal, but the picture is somewhat more complex than that described above.) Another diagnostic for coupling through imidazolates, however, is the EPR spectrum itself. For coupled species, the EPR signal is broad and, hence, quite distinct from mononuclear type 2 spectra such as those in Figure 3 (46–48). This unusual signal is also typically accompanied by a $\Delta M = 2$ half field transition (46–48). As noted in Results, however, we did not observe a half field transition, and the EPR spectra displayed in Figure 3 are characteristic of isolated Cu^{2+} ions and show no unusual broadening or dipolar splittings as would be expected for a coupled species. These combined observations suggest that there is no EPR evidence in support of an imidazolate bridged species in PrP(57–91) when bound to four Cu^{2+} ions.

In a recent Raman study of octarepeat-derived peptides, Miura et al. concluded that the segment **H**GGG is the fundamental Cu^{2+} binding unit at pH 7.4 (16,18). Further, their study indicated that the peptide coordinates Cu^{2+} via the N_π atom (also denoted Nδ1) of the histidine side chain and two deprotonated main chain amide nitrogens. Our findings are largely consistent with theirs, but we find evidence for two binding modes within the octarepeat. Further, a Trp residue following the **H**GGG binding unit is needed to reproduce the dominant spectral component of the multi-octarepeat peptides.

Together these data indicate that the majority of copper is bound within the segment **H**GGG and that each octarepeat segment binds copper independently. Component 1 in the EPR spectra of Figure 3 therefore arises from coordination of the histidine side chain nitrogen and two

deprotonated glycine amide nitrogens. Component 2 may then arise from a state in which one of the glycine amides has released Cu^{2+} and been replaced by an oxygen-containing ligand such as a backbone carbonyl or water. The presence of the tryptophan (or X) residue after the **H**GGG segment clearly plays a role in the equilibrium between these two binding modes.

Figure 11 shows our working model for the dominant (component 1) octarepeat binding mode. EPR is mainly sensitive to the equatorial coordination shown in the model, but we recognize that there are probably oxygens from water or hydroxide at the axial positions. Because the EPR spectrum of copper bound **H**GG still gives a component 1 spectrum, although reduced in intensity, we propose that along with the imidazole, the next two glycine amides participate in Cu^{2+} coordination. Crystal structures of peptide–Cu^{2+} complexes indeed show that coordination of sequential backbone amides is common (41, 42, 49). The EPR data also suggest that a residue following the **H**GGG segment (W or X) is necessary to give a dominant component 1 spectra, and we propose that this additional residue contributes an oxygen to the coordination environment. Thus, in our model, the Trp carbonyl is shown coordinating the metal ion center. Not only is this model consistent with our findings, but it also explains the near proximity of the Trp indole to the paramagnetic center demonstrated by fluorescence quenching experiments (15). Miura et al. have also proposed coordination by two amides (18), and our model is also consistent with their experimental data. Finally, we note that a crankshaft rearrangement of one of the first or second Gly to replace a coordinated amide nitrogen with a carbonyl may explain the component 2 spectrum that dominates at lower pH.

For a fully Cu^{2+} loaded protein, this model suggests that the metal ion binding sites in the N-terminal domain are like beads on a string where each bead is a Cu^{2+}-**H**GGGW segment separated by intervening Gly–Gln–Pro (GQP) links. Interestingly, Gly and Pro often participate in β-turns, and thus the intervening links may provide a mechanism for allowing the Cu^{2+} binding segments to fold and perhaps collapse together. If the model in Figure 11 proves to be correct, it will represent a novel Cu^{2+} binding site in proteins. Although serum albumin binds Cu^{2+} in a GG**H** segment via amide nitrogens (50), most copper binding proteins coordinate the metal ion through side chain functionalities (e.g., His, Cys, Met). Moreover, the proposed binding mode may figure nicely into current theories of PrP function. Cu^{2+} stimulates endocytosis (13), and it is proposed that PrP's role may be to sense the concentration of Cu^{2+} and shuttle the metal ion from the extracellular domain at pH > 7 to endo-lysosomes at reduced pH (19, 25). To support this hypothesis, PrP must exhibit pH-sensitive binding. Amide coordination to Cu^{2+} as shown in Figure 11 is extremely pH-sensitive. In the absence of Cu^{2+}, backbone amide pK_a's are in the range of 13 to 15. However, when Cu^{2+} is brought into proximity by coordination to a His side chain, the pK_a's of nearby amides are greatly reduced and often below 7 (51). At pH > 7 these amides readily deprotonate and coordinate Cu^{2+} through the nitrogen. However, if the pH is lowered by one or two units, protonation competes with Cu^{2+} coordination thereby lowering the affinity for the metal ion (52, 53). Figures 1 and 2 clearly reflect substantial pH sensitivity in the PrP octarepeat domain. In addition, ESI-MS of PrP(57–91) suggests that only two Cu^{2+} bind at pH 6 (19). The model proposed in Figure 11 accounts for differential Cu^{2+} affinity above and below pH = 7 and is consistent with current theories linking PrP function to Cu^{2+} shuttling through endocytosis.

CONCLUSION

These studies combined peptide design with EPR, ESEEM, CD spectroscopy, and titration experiments to evaluate the Cu^{2+} binding unit of the PrP N-terminus. The findings help resolve whether each Cu^{2+} binds within a single octarepeat (15,16,18) or between octarepeats via imidazolate bridging (17). The EPR studies further show that there are two binding modes at pH 7.4 where the dominant mode arises from coordination of three nitrogens. In addition, the way in which Cu^{2+} binds to the multi-octrapeat peptides appears to depend on the relative metal

ion and peptide concentrations. The simple peptide unit **H**GGGW possesses the necessary features to bind Cu^{2+} in a manner that is spectroscopically indistinguishable from the dominant binding mode observed for the multi-octarepeat peptides. Our observations are collected into a working model for binding above pH 7 where we propose that coordination in the equatorial plane arises from a nitrogen of the His imidazole, two backbone nitrogens from the following glycines, and the amide carbonyl of the tryptophan. Although this model needs further scrutiny, it provides a starting point for evaluating the metal ion induced structure of the PrP N-terminus and the mechanism by which PrP takes up and releases Cu^{2+}. Future work will also focus on elucidation of the component 2 binding mode, its possible physiological role, and how low pH leads to specific changes in the Cu^{2+} binding environment.

Acknowledgments

The authors are grateful to J. Viles, P. Mascharak, J. McNulty, and E. Solomon for helpful discussion and advice. Finally, we are grateful to J. Robertson, M. Carnevali, H. Rood, and O. Alvizo for help with peptide synthesis and some of the spectroscopic studies. This work is dedicated to the memory of Karen M. Lundberg (1955–1999).

REFERENCES

1. Prusiner SB. Science 1982;216:136–144. [PubMed: 6801762]
2. Prusiner SB. Science 1991;252:1515–1522. [PubMed: 1675487]
3. Prusiner SB. Science 1997;278:245–251. [PubMed: 9323196]
4. Zahn R, Liu A, Luhrs T, Riek R, von Schroetter C, Lopez Garcia F, Billeter M, Calzolai L, Wider G, Wuthrich K. Proc. Natl. Acad. Sci. U.S.A 2000;97:145–150. [PubMed: 10618385]
5. Riek R, Hornemann S, Wider G, Billeter M, Glockshuber R, Wuthrich K. Nature 1996;382:180–182. [PubMed: 8700211]
6. Riek R, Hornemann S, Wider G, Glockshuber R, Wuthrich K. FEBS Lett 1997;413:282–288. [PubMed: 9280298]
7. Donne DG, Viles JH, Groth D, Mehlhorn I, James TL, Cohen FE, Prusiner SB, Wright PE, Dyson HJ. Proc. Natl. Acad. Sci. U.S.A 1997;94:13452–13456. [PubMed: 9391046]
8. James TL, Liu H, Nikolai BU, Farr-Lones S, Zhang H, Donne DG, Kaneko K, Groth D, Melhorn I, Prusiner SB, Cohen FE. Proc. Natl. Acad. Sci. U.S.A 1997;94:10086–10091. [PubMed: 9294167]
9. Pan K-M, Baldwin M, Nguyen J, Gasset M, Serban A, Groth D, Mehlhorn I, Huang Z, Fletterick RJ, Cohen FE, Prusiner SB. Proc. Natl. Acad. Sci. U.S.A 1993;90:10962–10966. [PubMed: 7902575]
10. Safar J, Roller PP, Gadjdusek DC, Gibbs CJJ. J. Biol. Chem 1993;268:20276–20284. [PubMed: 8104185]
11. Brown DR, Qin K, Herms JW, Madlung A, Manson J, Strome R, Fraser PE, Kruck T, von Bohlen A, Schulz-Schaeffer W, Giese A, Westway D, Kretzschmar H. Nature 1997;390:684–687. [PubMed: 9414160]
12. Brown DR, Schmidt B, Kretzschmar HA. J. Neurochem 1998;70:1686–1693. [PubMed: 9523587]
13. Pauly PC, Harris DA. J. Biol. Chem 1998;273:33107–33119. [PubMed: 9837873]
14. Hornshaw MP, McDermott JR, Candy JM. Biochem. Biophys. Res. Commun 1995;207:621–629. [PubMed: 7864852]
15. Stöckel J, Safar J, Wallace AC, Cohen FE, Prusiner SB. Biochemistry 1998;37:7185–7193. [PubMed: 9585530]
16. Miura T, Hori-i A, Takeuchi H. FEBS Lett 1996;396:248–252. [PubMed: 8914996]
17. Viles JH, Cohen FE, Prusiner SB, Goodin DB, Wright PE, Dyson HJ. Proc. Natl. Acad. Sci. U.S.A 1999;96:2042–2047. [PubMed: 10051591]
18. Miura T, Hori-i A, Mototani H, Takeuchi H. Biochemistry 1999;38:11560–11569. [PubMed: 10471308]
19. Whittal RM, Ball HL, Cohen FE, Burlingame AL, Prusiner SB, Baldwin MA. Protein Sci 2000;9:332–343. [PubMed: 10716185]

20. Gabriel J-M, Oesch B, Kretzschmar H, Scott M, Prusiner SB. Proc. Natl. Acad. Sci. U.S.A 1992;89:9097–9101. [PubMed: 1409608]
21. Wopfner F, Weidenhofer G, Schneider R, von Brunn A, Gilch S, Schwarz TF, Werner T, Schatzl HM. J. Mol. Biol 1999;289:1163–1178. [PubMed: 10373359]
22. Sulkowski E. FEBS Lett 1992;307:129–130. [PubMed: 1353727]
23. Brown DR, Wong B-S, Hafiz F, Clive C, Haswell SJ, Jones IM. Biochem. J 1999;344:1–5. [PubMed: 10548526]
24. Herms J, Tings T, Gall S, Madlung A, Giese A, Siebert H, Schürmann P, Windl O, Brose N, Kretzschmar H. J. Neurosci 1999;19:8866–8875. [PubMed: 10516306]
25. Waggoner DJ, Drisaldi B, Bartnikas TB, Casareno RLB, Prohaska JR, Gitlin JD, Harris DA. J. Biol. Chem 2000;275:7455–7458. [PubMed: 10713045]
26. Jiang F, McCracken J, Peisach J. J. Am. Chem. Soc 1990;112:9035–9044.
27. Bender CJ, Casimiro DR, Peisach J, Dyson HJ. J. Chem. Soc., Faraday Trans 1997;93:3967–3980.
28. Cornelius JB, McCracken J, Clarkson RB, Belford RL, Peisach J. J. Phys. Chem 1990;94:6977–6982.
29. Peisach J, Blumberg WE. Arch. Biochem. Biophys 1974;165:691–708. [PubMed: 4374138]
30. Allendorf MD, Spira DJ, Solomon EI. Proc. Natl. Acad. Sci. U.S.A 1985;82:3063–3067. [PubMed: 2987909]
31. Safar J, Wille H, Itri V, Groth D, Serban H, Torchia M, Cohen FE, Prusiner SB. Nat. Med 1998;4:1157–1165. [PubMed: 9771749]
32. Mims, WB.; Peisach, J. Biological Magnetic Resonance. Berliner, LJ.; Reuben, J., editors. New York: Plenum Press; 1981.
33. Mims WB, Peisach J. J. Chem. Phys 1978;69:4921–4930.
34. Flanagan HL, Singel DJ. J. Chem. Phys 1987;87:5606–5616.
35. McCracken J, Pember S, Benkovic SJ, Villafranca JJ, Miller RJ, Peisach J. J. Am. Chem. Soc 1988;110:1069–1074.
36. Froncisz W, Hyde JS. J. Chem. Phys 1980;73:3123–3131.
37. Yuan H, Collins MLP, Antholine WE. J. Am. Chem. Soc 1997;119:5073–5074.
38. Yuan H, Antholine WE, Kroneck PMH. J. Inorg. Biochem 1998;71:99–107. [PubMed: 9755494]
39. Antholine WE, Hyde JS, Sealy RC, Petering DH. J. Biol. Chem 1984;259:4437–4440. [PubMed: 6200482]
40. Antholine W, Taketa F. J. Inorg. Biochem 1982;16:145–154. [PubMed: 6281382]
41. Freeman HC, Schoone JC, Sime JG. Acta Crystallogr 1965;18:381–392.
42. Freeman HC, Taylor MR. Acta Crystallogr 1965;18:939–952. [PubMed: 14298284]
43. Pogni R, Baratto MC, Busi E, Basosi R. J. Inorg. Biochem 1999;73:157–165. [PubMed: 10331245]
44. Parge HE, Hallewell RA, Tainer JA. Proc. Natl. Acad. Sci. U.S.A 1992;89:6109–6113. [PubMed: 1463506]
45. Hough MA, Hasnain SS. J. Mol. Biol 1999;287:579–592. [PubMed: 10092461]
46. Kolks G, Lippard SJ, Waszczak JV, Lilienlthal HR. J. Am. Chem. Soc 1982;104:717–725.
47. Chaudhuri P, Karpenstein I, Winter M, Lengen M, Butzlaff C, Bill E, Trautwein AX, Flörke U, Haupt H-J. Inorg. Chem 1993;32:888–894.
48. Strothkamp KG, Lippard SJ. Biochemistry 1981;20:7488–7493. [PubMed: 7326242]
49. Camerman N, Camerman A, Sarkar B. Can. J. Chem 1976;54:1309–1316.
50. Lau SJ, Kruck TP, Sarkar B. J. Biol. Chem 1974;249:5878–5884. [PubMed: 4411707]
51. Sundberg RJ, Martin RB. Chem. Rev 1974;74:471–517.
52. Bryce GF, Roeske RW, Gurd FR. J. Biol. Chem 1965;240:3837–3846. [PubMed: 5842056]
53. Bryce GF, Gurd FR. J. Biol. Chem 1966;241:122–129. [PubMed: 5901043]

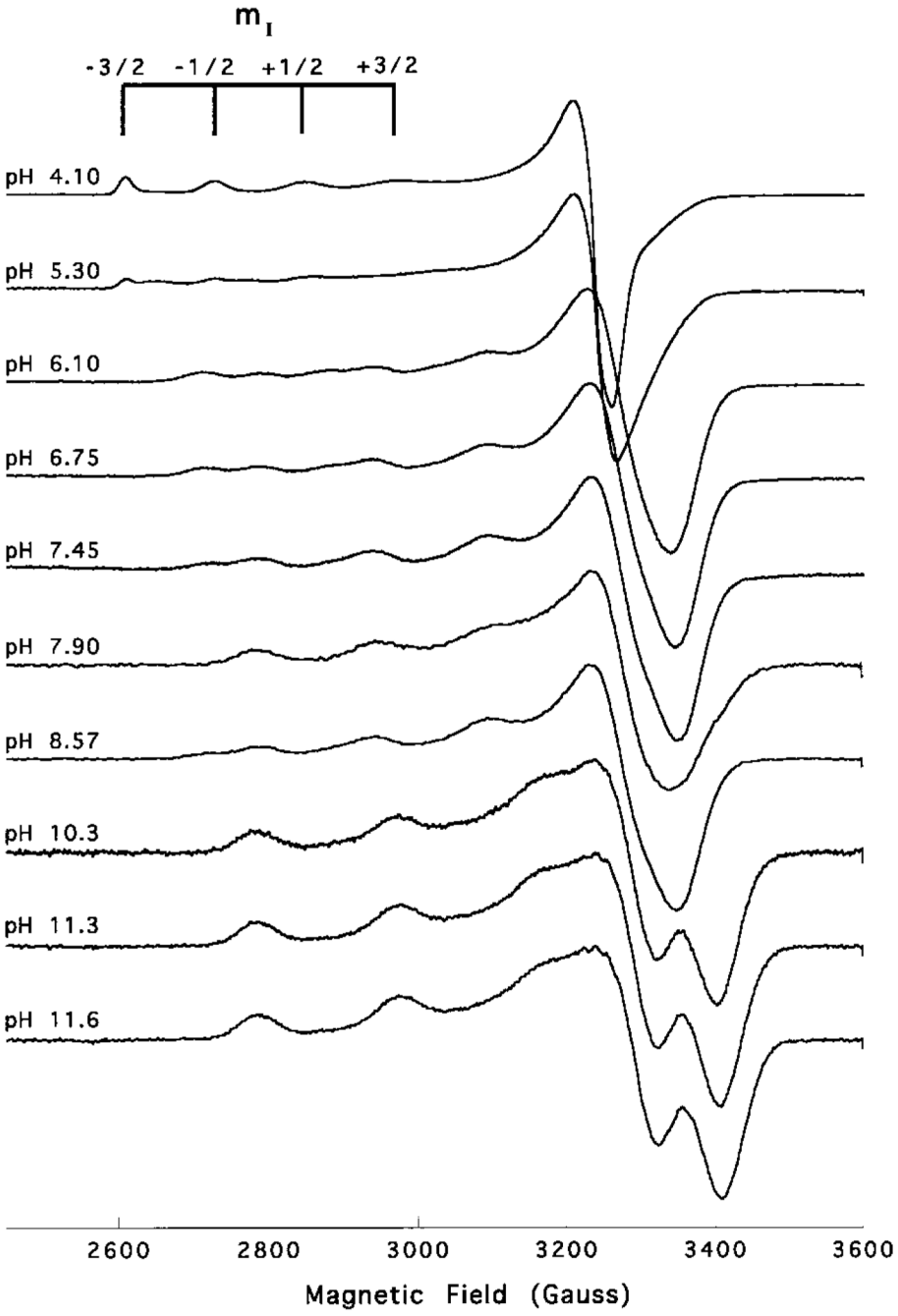

Figure 1.

X-band EPR spectra of $^{63}Cu^{2+}$ loaded PrP(23–28, 57–91) at different pH values. The grid at top identifies the four hyperfine lines arising from coupling to the ^{63}Cu (I = 3/2) nucleus. All spectra were collected at 77 K, ν_o = 9.43 GHz, and a sweep width of 1200 G.

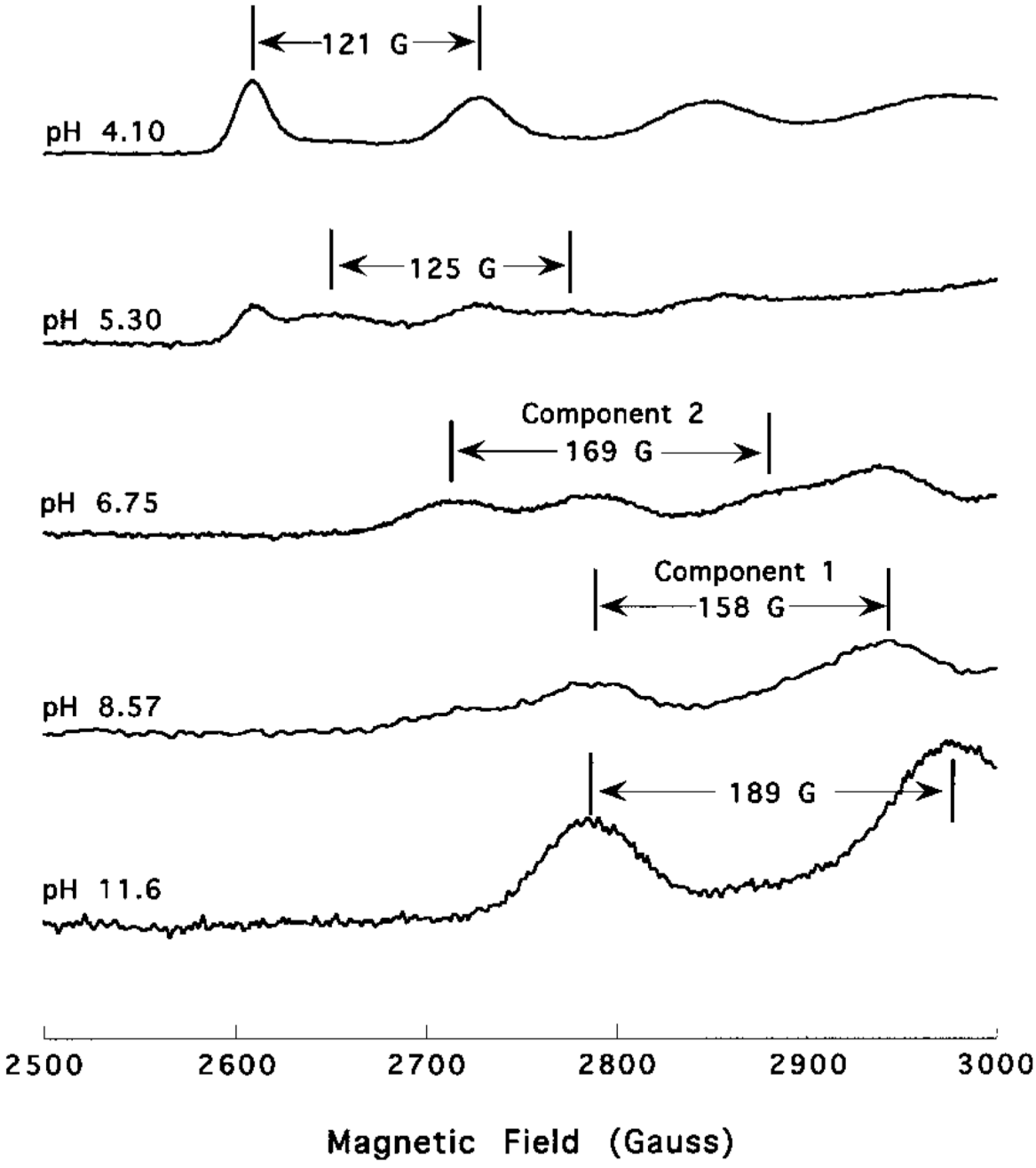

Figure 2.
Expansion of the low field (parallel) region from Figure 1 at selected pH values. As the pH increases there are marked changes of the four hyperfine lines reflecting changes in the ligand environment of the copper ion. Distinct species apparent at various points in the pH range are indicated.

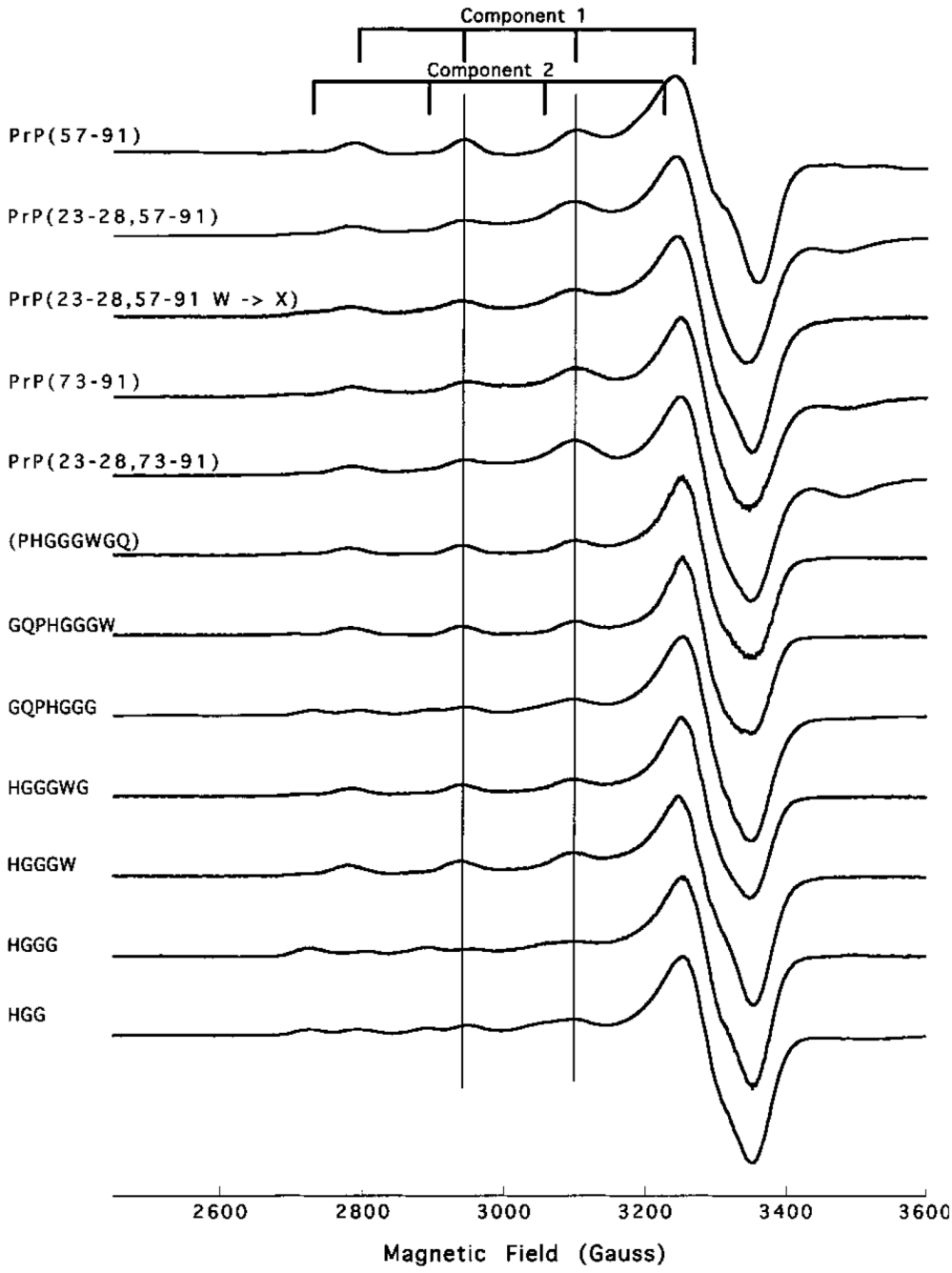

Figure 3.

X-band EPR spectra of all $^{63}Cu^{2+}$/peptide complexes at pH values 7.45 ± 0.07. Spectral component 1 and component 2 are indicated with grids at top. Vertical lines have been added to the $m_I = -1/2$ and $m_I = +1/2$ hyperfine lines of component 1 to aid in comparison of $g_{\|}$ and $A_{\|}$ values between complexes. All spectra collected at 77 K, $\nu_o = 9.43$ GHz, and a sweep width of 1200 G.

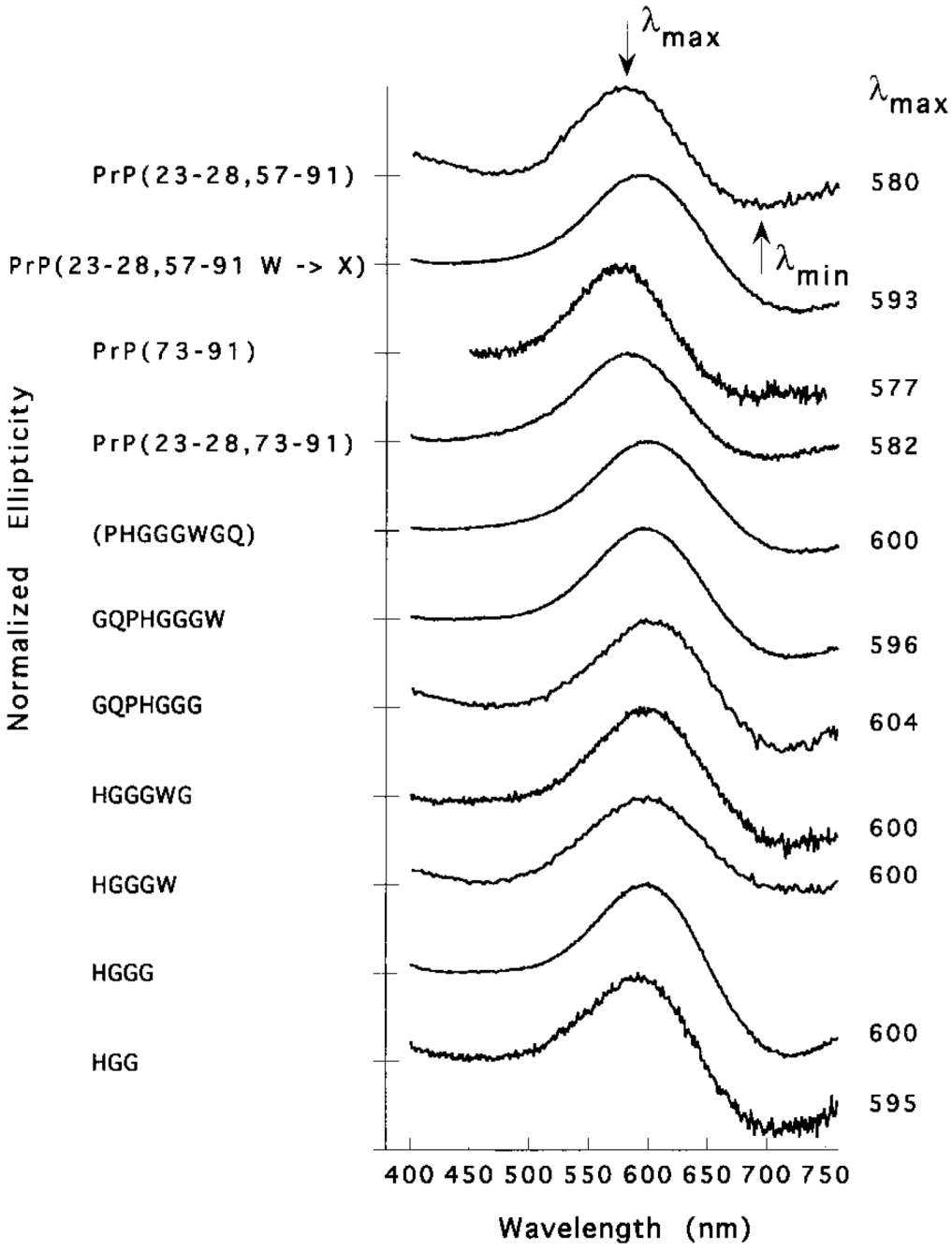

Figure 4.

Visible region CD spectra of all Cu^{2+}/peptide complexes at pH 7.4. The spectra are normalized along the *y* axis for comparison of λ_{max} and λ_{min}. The approximate baseline for each spectrum is indicated by hatch marks at the left. The λ_{max} of the positive CD band is listed to the right of each spectrum. Because of poor solubility, PrP(57–91) is not included in this figure. All spectra collected at 298 K.

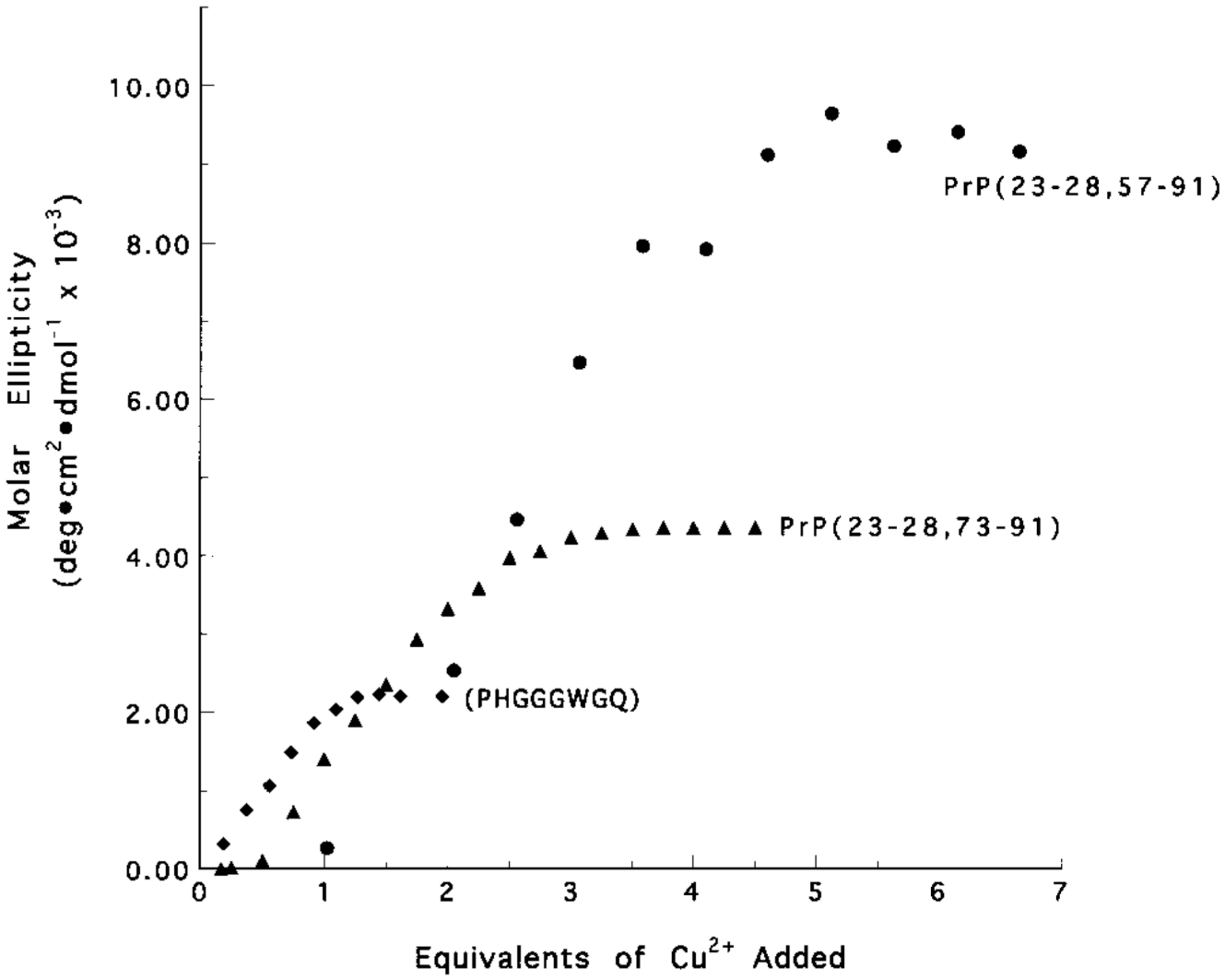

Figure 5.

CD signal intensity at λ_{max} as a function of titrated Cu^{2+} at pH 7.4 for the octarepeat, PrP(23–28, 73–91), and PrP(23–28, 57–91). Peptide concentrations are 398, 333, and 51 μM, respectively, and copper ion concentrations are reported in equivalents per peptide.

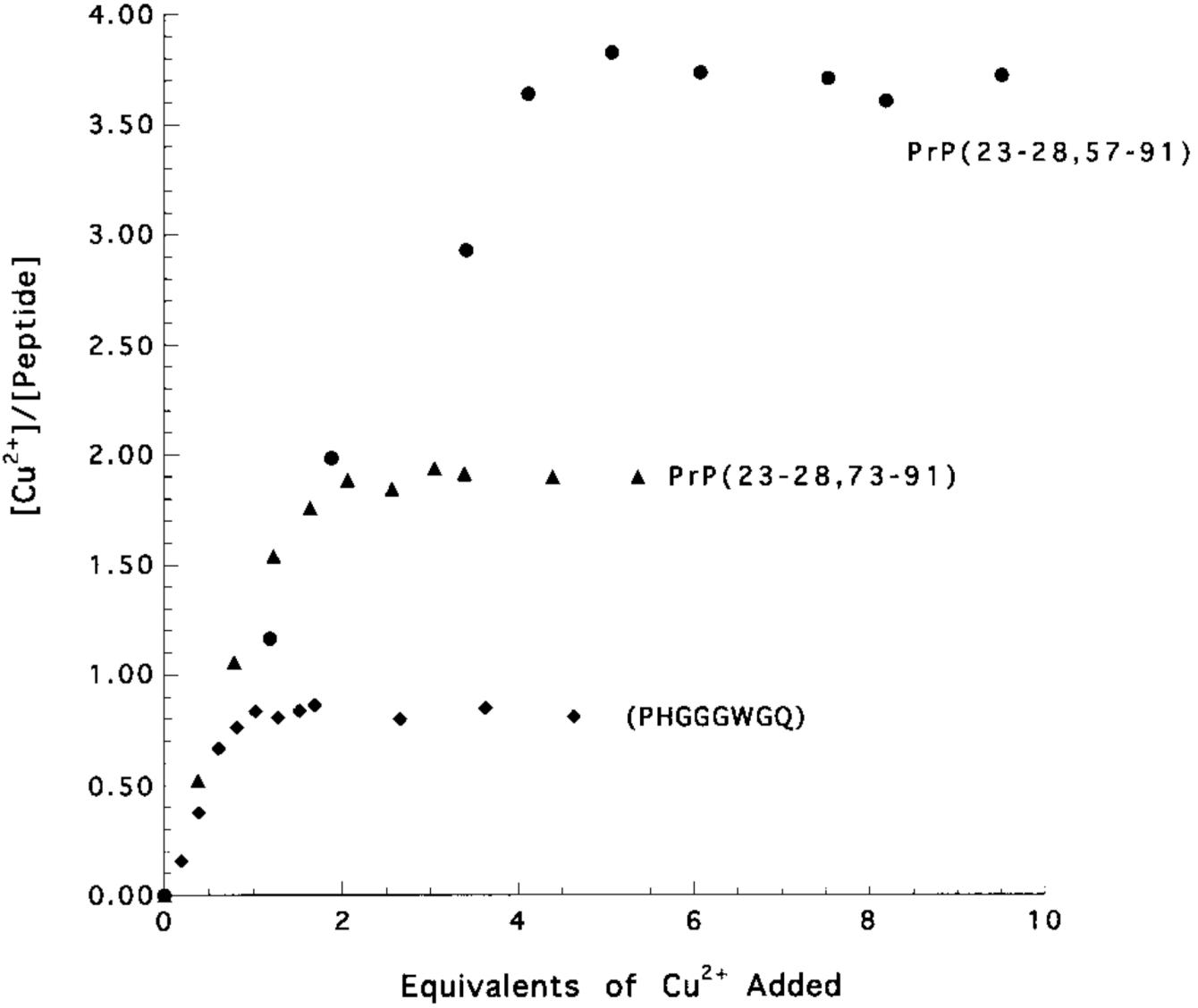

Figure 6.

Integrated EPR signal intensity as a function of titrated Cu^{2+} at pH 7.4 for the octarepeat, PrP (23–28, 73–91), and PrP-(23–28, 57–91). Peptide concentrations are 1000, 500, and 250 μM, respectively, and the copper ion concentration is reported in equivalents per peptide. All spectra collected at 298 K.

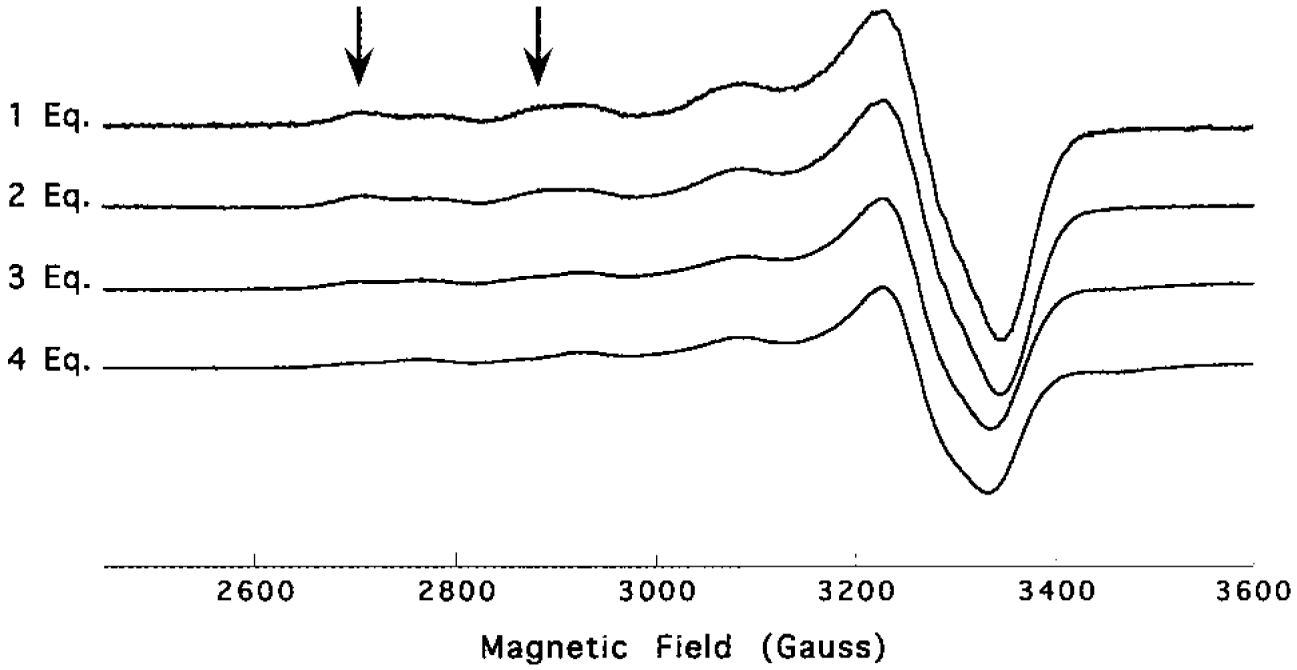

Figure 7.

X-band EPR spectra of 133 μM PrP(23–28, 57–91) with 1, 2, 3, and 4 equiv of Cu^{2+} at pH 7.4. Each spectrum has been normalized to unit area. Arrows have been added above the $m_I = -3/2$ and $m_I = -1/2$ hyperfine lines to highlight changes in this region. All spectra collected at 77 K, ν_o = 9.43 GHz, and a sweep width of 1200 G.

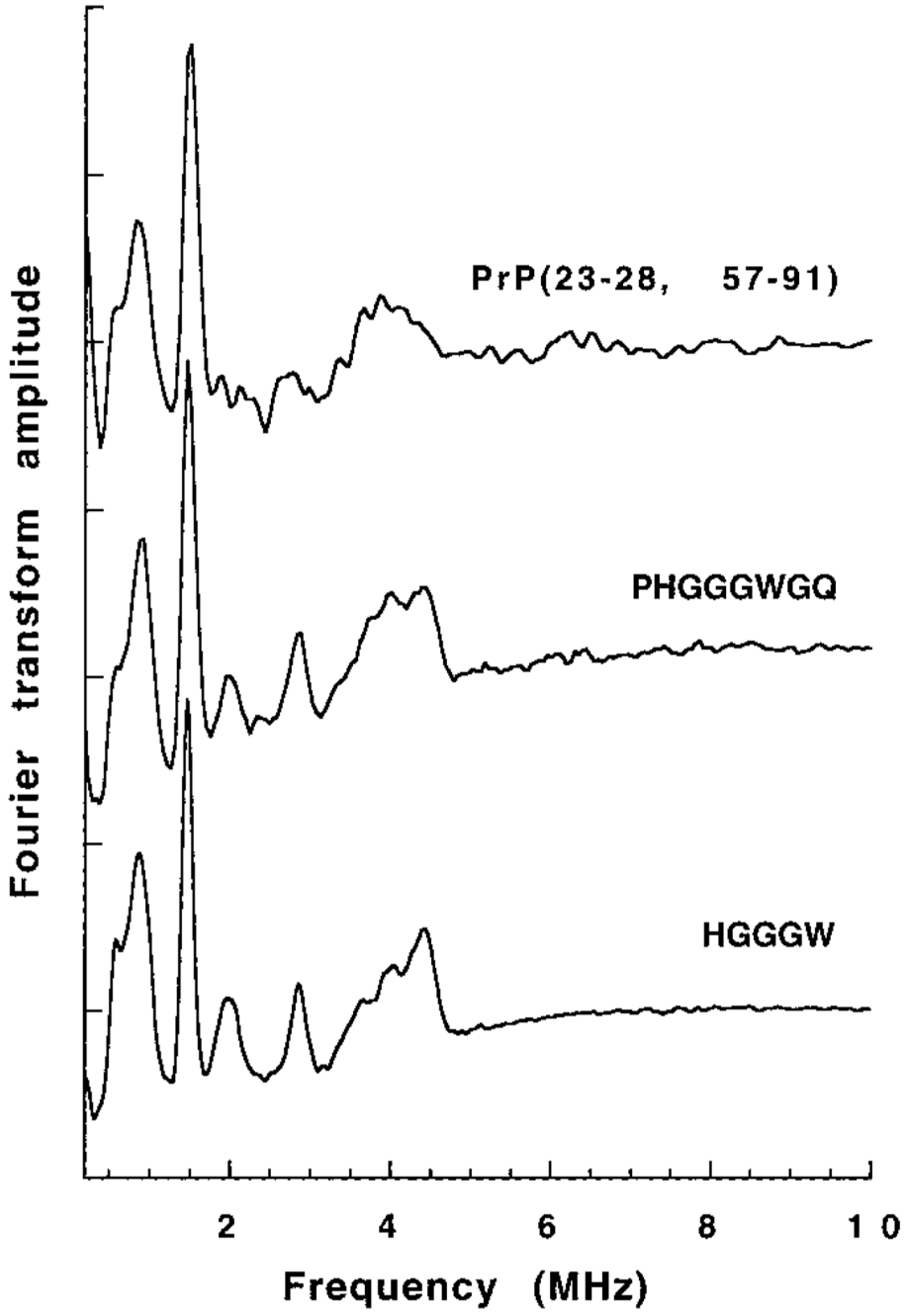

Figure 8.
Three pulse ESEEM spectra for PrP(23–28, 57–91), the octarepeat (P**H**GGGWGQ) and **H**GGGW obtained at X-band. Spectra were obtained at 4.2 K from the $g_{\perp}$ region of the spectrum with τ = 150 ns.

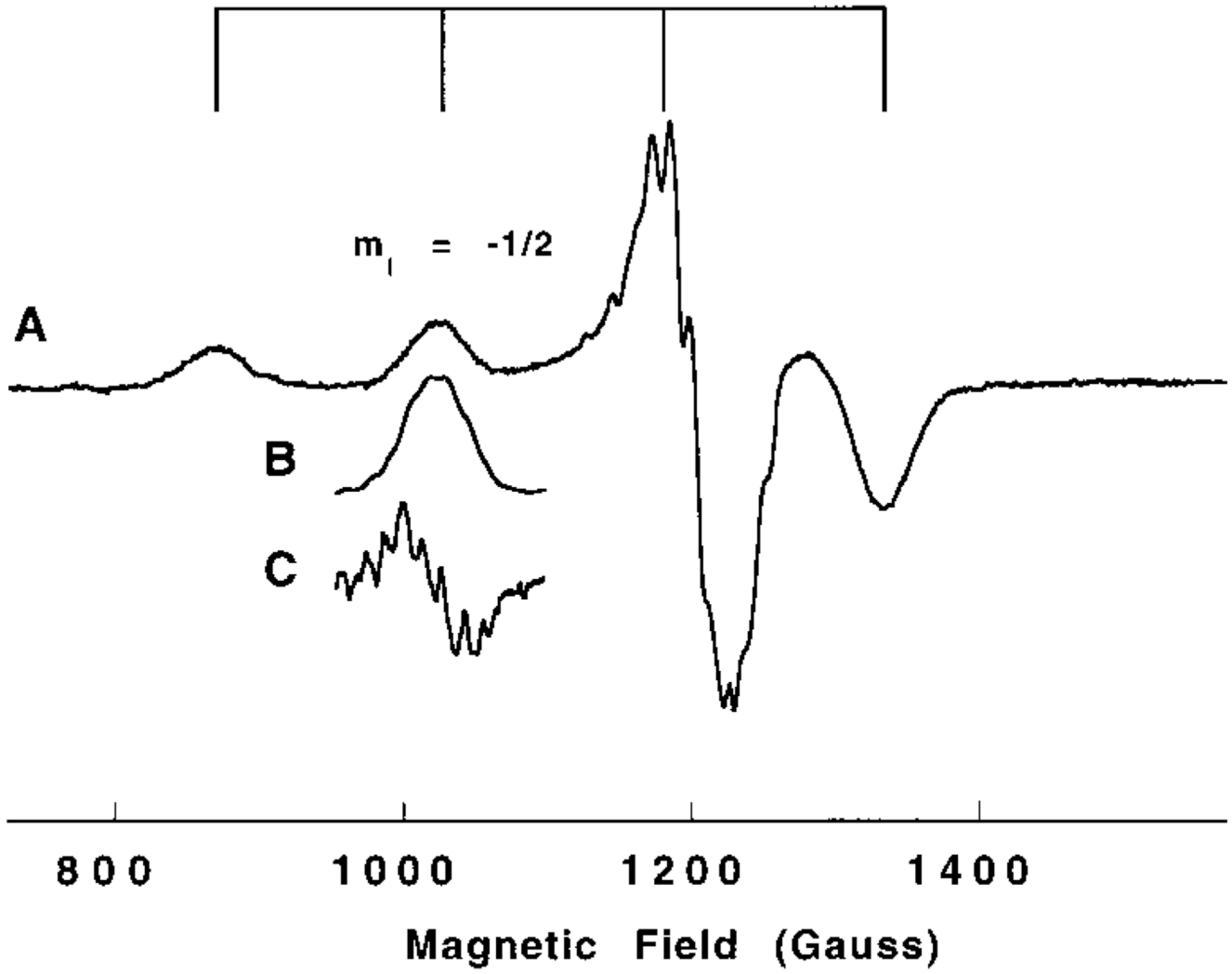

Figure 9.
S-band EPR (3.5 GHz) of the octarepeat (P**H**GGG-WGQ). The grid at the top shows the ^{63}Cu hyperfine splitting, and the $m_I = -1/2$ line is indicated. Trace A is the full field scan; trace B is the $m_I = -1/2$ line scanned with high resolution and signal averaging; trace C is the derivative of B emphasizing the multiplet structure.

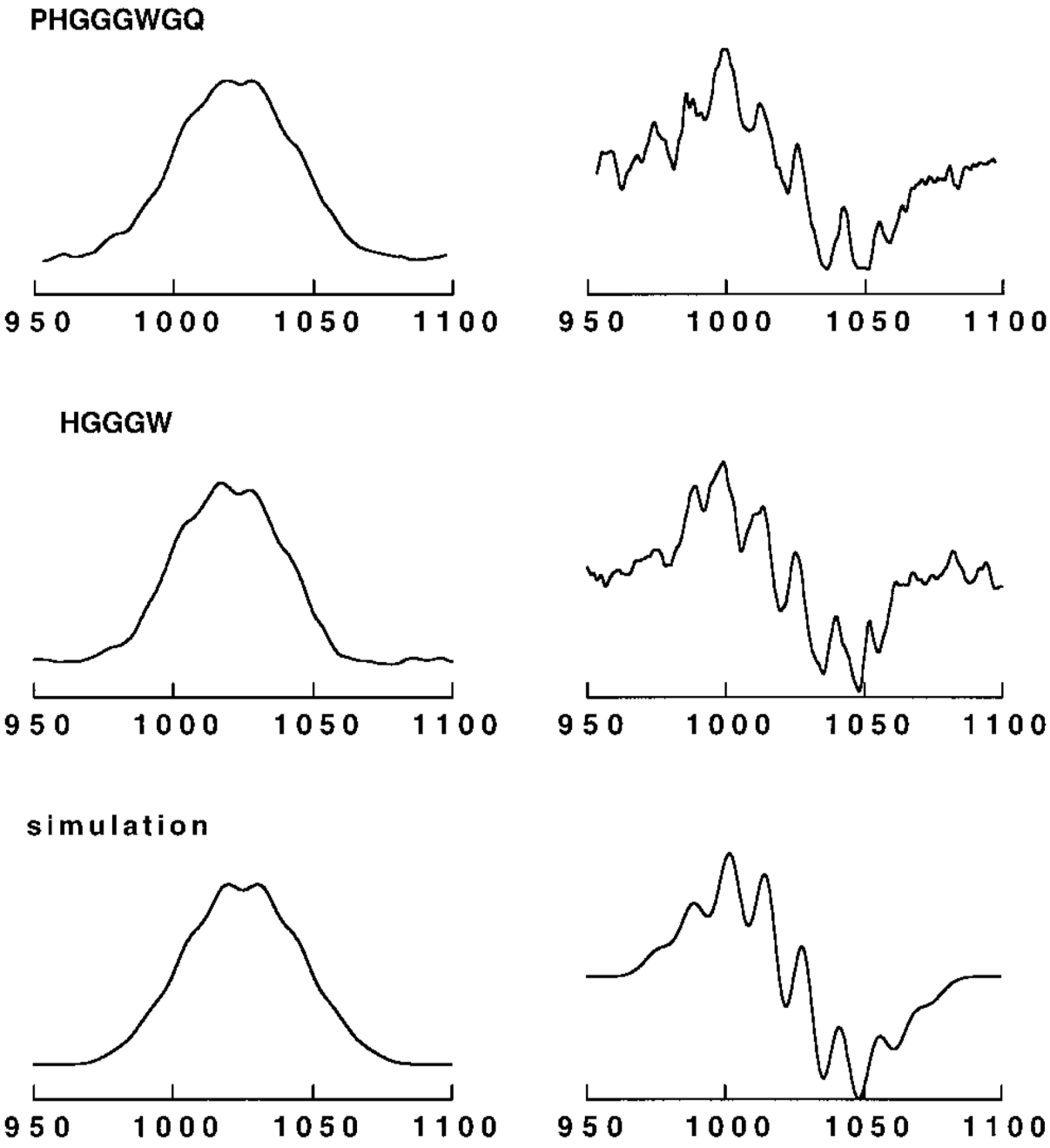

Figure 10.

Expansion of the $m_I = -1/2$ lines of the S-band EPR spectra. The octarepeat (P**H**GGGWGQ) and **H**GGGW lines are shown (left) along with their derivatives (right). The simulated spectrum is from a model of three equivalent nitrogens (a_N = 13 G) and one proton (a_H = 10 G).

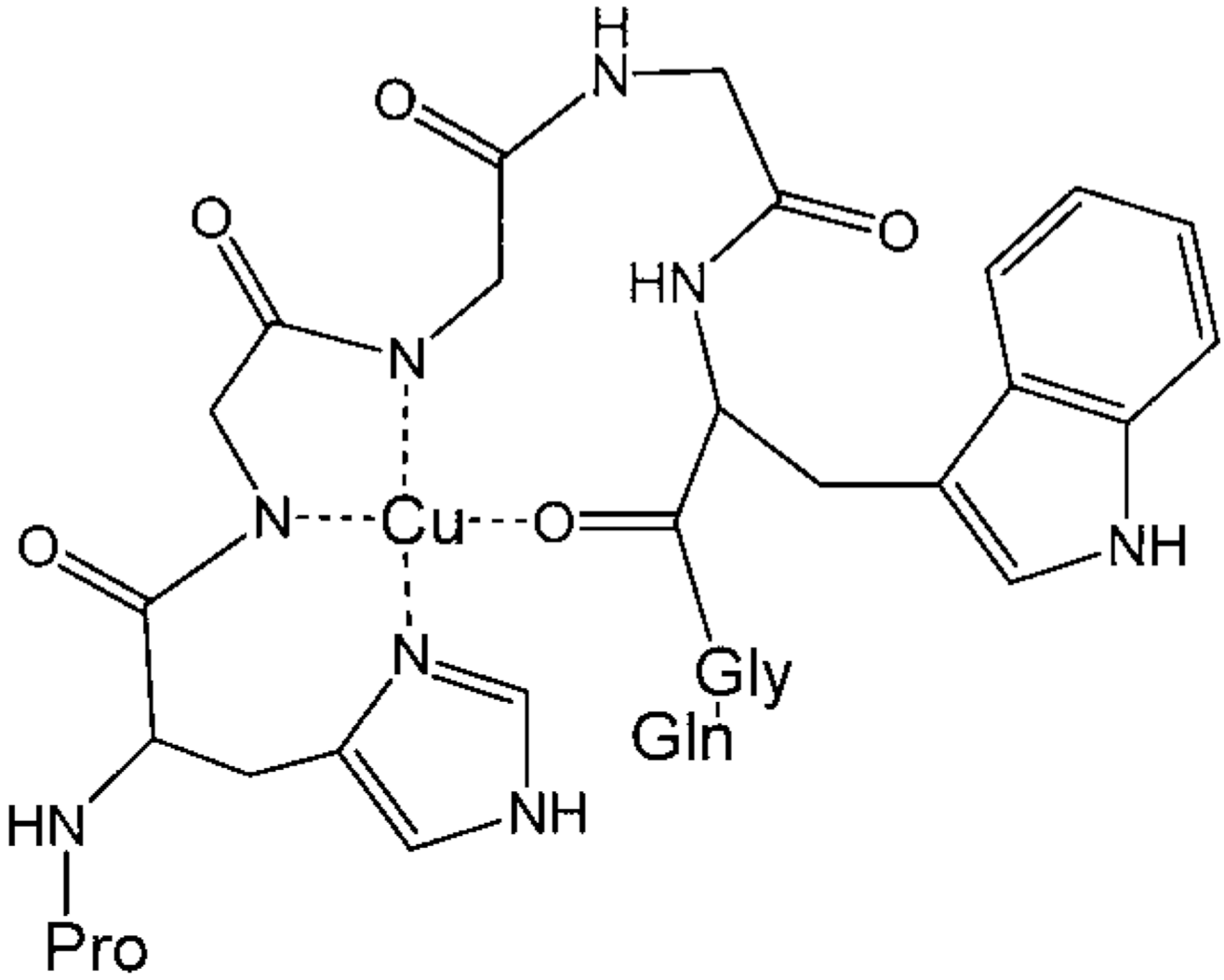

Figure 11.
Proposed bond-line model of the dominant binding mode (component 1) of the octarepeat segment (P**H**GGGWGQ).

Table 1

PrP-Derived Peptide Sequences

PrP(57–91)	WGQP**H**GGGWGQP**H**GGGWGQP**H**GGGWGQP**H**GGGWGQ
PrP(23–28, 57–91)	KKRPKPWGQP**H**GGGWGQP**H**GGGWGQP**H**GGGWGQP**H**GGGWGQ
PrP(23–28, 57–91 W→X)	KKRPKPXGQP**H**GGGXGQP**H**GGGXGQP**H**GGGXGQP**H**GGGXGQ
PrP(73–91)	P**H**GGGWGQP**H**GGGWGQ
PrP(23–28, 73–91)	KKRPKPWGQP**H**GGGWGQP**H**GGGWGQ
Octarepeat	P**H**GGGWGQ
	GQP**H**GGGW
	GQP**H**GGG
	HGGGWG
	HGGGW
	HGGG
	HGG

Table 2

EPR Parameters for $^{63}Cu^{2+}$ Loaded PrP(23–28, 57–91) at Different pH Values (cf. Figures 1 and 2)

		$A_{\parallel}$[b]			
pH	$g_{\parallel}$[a]	MHz	(G)	$g_{\perp}$[a]	ligating atoms
4.10	2.41	408	(121)	2.09	4 O
5.30	2.37	415	(125)	2.08	3 O, 1 N
6.75	2.27	537	(169)	2.06	2 O, 2 N
7.45	2.23	493	(158)	2.06	1 O, 3 N
8.57	2.23	493	(158)	2.06	1 O, 3 N
11.60	2.20	582	(189)	2.05	4 N

[a] The error in all reported *g*-values is less than ± 0.01.

[b] Error in A values ± 6 MHz (± 2 G).

Table 3

EPR Parameters for All $^{63}Cu^{2+}$/Peptide Complexes at pH values 7.45 ± 0.07 (cf. Figure 3)

sequence @ pH values 7.45 ± 0.07	component 1			component 2		
		$A_{\parallel}$[b]			$A_{\parallel}$[b]	
	$g_{\parallel}$[a]	MHz	(G)	$g_{\parallel}$[a]	MHz	(G)
PrP(57–91)	2.23	490	(157)			
PrP(23–28, 57–91)	2.23	493	(158)			
PrP(23–28, 57–91 W → X)	2.23	490	(157)			
PrP(73–91)	2.23	495	(159)			
PrP(23–28, 73–91)	2.23	493	(158)			
PHGGGWGQ	2.23	499	(160)			
GQPHGGGW	2.23	493	(158)			
GQPHGGG	2.23	472	(151)	2.26	535	(169)
HGGGWG	2.23	492	(157)			
HGGGW	2.23	496	(159)			
HGGG	2.23	461	(148)	2.26	525	(166)
HGG	2.23	473	(152)	2.26	524	(166)

[a] The error in all reported *g*-values is less than ± 0.01.

[b] Error in A values ± 6 MHz (± 2 G).

Table 4

Summary of EPR and CD Titration Data for the Octarepeat, PrP(23–28, 73–91), and PrP(23–28, 57–91) (cf. Figures 5 and 6)

	octarepeat (equiv)	PrP(23–28, 73–91) (equiv)	Prp(23–28, 57–91) (equiv)
max EPR signal intensity[a]	0.92	1.90	4.24
Cu^{2+} conc detected by EPR[b]	0.83	1.88	3.83
max CD molar ellipticity[c]	1.06	2.53	4.37
normalized CD molar ellipticity[d]	1.00	2.00	4.19

[a] Equivalents of Cu^{2+} added to achieve maximum EPR signal intensity.

[b] Absolute bound Cu^{2+} concentration detected by EPR.

[c] Equivalents of Cu^{2+} added to achieve maximum CD molar ellipticity.

[d] Maximum molar ellipticity scaled as integer value of octarepeat molar ellipticity when fully loaded with Cu^{2+}.